Mutations in *HID1* Cause Syndromic Infantile Encephalopathy and Hypopituitarism

Anne Schänzer, MD ,[1†] Melanie T. Achleitner, MSc,[2†] Dietrich Trümbach, PhD ,[3,4] Laurence Hubert, MSc ,[5] Arnold Munnich, MD, PhD ,[5] Barbara Ahlemeyer, PhD,[6] Maha M. AlAbdulrahim, MSc,[7] Philipp A. Greif, MD ,[8] Sebastian Vosberg, PhD ,[8,9] Blake Hummer, PhD,[10] René G. Feichtinger, PhD ,[2] Johannes A. Mayr, PhD,[2] Saskia B. Wortmann, MD, PhD,[2,11] Heidi Aichner, MD,[12] Sabine Rudnik-Schöneborn, MD,[13] Anna Ruiz, PhD ,[14] Elisabeth Gabau, MD ,[15] Jacobo Pérez Sánchez, MD ,[15] Sian Ellard, PhD ,[16,17] Tessa Homfray, MD,[18] Karen L. Stals, BSc,[16] Wolfgang Wurst, PhD ,[3,19,20,21] Bernd A. Neubauer, MD,[22] Till Acker, MD ,[1] Stefan K. Bohlander, MD,[23] Cédric Asensio, PhD,[10] Claude Besmond, PhD ,[5] Fowzan S. Alkuraya, MD ,[24] Moenaldeen D. AlSayed, MD,[25] Andreas Hahn, MD ,[22‡] and Axel Weber, MD [26‡]

Address correspondence to Dr Axel Weber, Institute of Human Genetics, Schlangenzahl 14, 35392 Giessen, Germany. E-mail: axel.weber@humangenetik. med.uni-giessen.de. Prof Anne Schänzer, Institute of Neuropathology, Justus-Liebig-University, Giessen, Germany. E-mail: anne.schaenzer@patho.med. uni-giessen.de

†These authors contributed equally to this work.

‡These authors shares the senior authorship and contributed equally to this work.

From the [1]Institute of Neuropathology, Justus-Liebig-University, Giessen, Germany; [2]University Children's Hospital, Paracelsus Medical University (PMU), Salzburg, Austria; [3]Institute of Developmental Genetics, Helmholtz Center, Munich, Germany; [4]Institute of Metabolism and Cell Death, Helmholtz Center, Munich, Germany; [5]Inserm UMR1163, Imagine Institute, Translational Genetics, Université de Paris, Paris, France; [6]Institute for Anatomy and Cell Biology, Division of Medical Cell Biology, Justus Liebig University, Giessen, Germany; [7]King Abdullah Bin Abdulaziz University Hospital, Riyadh, Saudi Arabia; [8]Experimental Leukemia and Lymphoma Research Department of Medicine III, University Hospital, LMU Munich, Munich, Germany; [9]German Cancer Research Centre (DKFZ), Heidelberg, Germany; [10]Molecular and Cellular Biophysics Program, Department of Biological Sciences, University of Denver, Denver, CO, USA; [11]Radboud Center for Mitochondrial Medicine, Department of Pediatrics, Amalia Children's Hospital, Radboudumc, Nijmegen, The Netherlands; [12]Department of Pediatrics, Academic Teaching Hospital, Landeskrankenhaus Feldkirch, Feldkirch, Austria; [13]Division of Human Genetics, Medical University of Innsbruck, Innsbruck, Austria; [14]Genetics Laboratory, UDIAT-Centre Diagnòstic, Parc Taulí Hospital Universitari, Institut d'Investigació i Innovació Parc Taulí I3PT, Universitat Autònoma de Barcelona, Sabadell, Spain; [15]Paediatric Unit, Parc Taulí Hospital Universitari, Institut d'Investigació i Innovació Parc taulí I3PT, Universitat Autònoma de Barcelona, Sabadell, Spain; [16]Genomic Laboratory, Royal Devon & Exeter NHS Foundation Trust, Exeter, UK; [17]College of Medicine and Health, University of Exeter, Exeter, UK; [18]Saint George's University Hospital and Royal Brompton Hospital, London, UK; [19]Chair of Developmental Genetics, Faculty of Life and Food Sciences Weihenstephan, Technische Universität München, Freising-Weihenstephan, Germany; [20]Deutsches Zentrum für Neurodegenerative Erkrankungen e. V. (DZNE), Munich, Germany; [21]Munich Cluster for Systems Neurology (SyNergy), Ludwig-Maximilians-Universität, Munich, Germany; [22]Department of Child Neurology, Justus-Liebig-University, Giessen, Germany; [23]Leukaemia and Blood Cancer Research Unit, Department of Molecular Medicine and Pathology, The University of Auckland, Auckland, New Zealand; [24]Department of Translational Genomics, Center for Genomic Medicine, King Faisal Specialist Hospital and Research Center, Riyadh, Saudi Arabia; [25]Department of Medical Genetics, King Faisal Specialist Hospital and Research Center, Riyadh, Saudi Arabia; and [26]Institute of Human Genetics, Justus-Liebig-University, Giessen, Germany

Additional supporting information can be found in the online version of this article.

Objective: Precursors of peptide hormones undergo posttranslational modifications within the trans-Golgi network (TGN). Dysfunction of proteins involved at different steps of this process cause several complex syndromes affecting the central nervous system (CNS). We aimed to clarify the genetic cause in a group of patients characterized by hypopituitarism in combination with brain atrophy, thin corpus callosum, severe developmental delay, visual impairment, and epilepsy.

Methods: Whole exome sequencing was performed in seven individuals of six unrelated families with these features. Postmortem histopathological and HID1 expression analysis of brain tissue and pituitary gland were conducted in one patient. Functional consequences of the homozygous *HID1* variant p.R433W were investigated by Seahorse XF Assay in fibroblasts of two patients.

Results: Bi-allelic variants in the gene *HID1 domain-containing protein 1* (*HID1*) were identified in all patients. Postmortem examination confirmed cerebral atrophy with enlarged lateral ventricles. Markedly reduced expression of pituitary hormones was found in pituitary gland tissue. Colocalization of HID1 protein with the TGN was not altered in fibroblasts of patients compared to controls, while the extracellular acidification rate upon stimulation with potassium chloride was significantly reduced in patient fibroblasts compared to controls.

Interpretation: Our findings indicate that mutations in *HID1* cause an early infantile encephalopathy with hypopituitarism as the leading presentation, and expand the list of syndromic CNS diseases caused by interference of TGN function.

The secretion of neurotransmitters and hormones is mandatory for intercellular communication either directly, for example between neuronal cells in close proximity or over distance *via* the circulating blood as a carrier for the information. Prior to the release at the cellular surface, precursors of neuropeptides and peptide hormones undergo several posttranslational modifications and are sorted into different types of vesicles within the trans-Golgi network (TGN). The final step of the secretory pathway is a well-coordinated fusion of loaded vesicles with the plasma membrane.[1]

HID1 domain-containing protein 1 (HID1, MIM*605752) is a protein involved in vesicle trafficking within the TGN, but has not yet been linked to human disease. The gene *High-temperature induced dauer formation 1* (*Hid-1*) was described for the first time in the nematode *Caenorhabditis elegans* associated with formation of arrested third stage larvae named "dauers" in response to high-temperature culture conditions.[2] *Hid-1* mutants display altered dauer formation, uncoordinated locomotion, constipation, and egg laying defects.[2] In *C. elegans*, neuronal HID-1 resides on intracellular membranes in neuronal cell soma and is involved in aspects of biogenesis, maturation, or trafficking of dense core vesicles (DCVs) within axons to synaptic regions.[3] HID1 localizes to the cytosolic medial- and trans-Golgi apparatus and a N-terminal myristoylation domain is required for HID1 binding to the TGN.[3,4] Loss of HID1 impairs TGN function in a mammal cell system.[5]

Pathogenic genetic variants affecting proteins involved at different steps of the TGN secretory pathway are known to cause several complex syndromes comprising severe intellectual disability, epilepsy and brain anomalies early in life like, for example, Early infantile epileptic encephalopathy-4 (EIEE4, MIM#612164),[6] Warburg-Micro syndrome (MIM#600118, MIM#614225),[7] Martsolf syndrome (MIM#212720),[8] Smith-McCort dysplasia 2 (SMC2, MIM#615222),[9] Dyggve-Melchior-Clausen disease (DMC, MIM#223800) and Smith-McCort dysplasia 1 (SMC1, MIM#607326).[10,11]

Here, we report on seven patients from six unrelated families with hypopituitarism and early infantile encephalopathy, in whom we identified bi-allelic mutations in *HID1*, and provide evidence for their functional consequences.

Subjects and Methods

Subjects

HID1 mutations were independently identified by exome sequencing performed through clinical care and evaluated as probably disease causing in seven patients of six unrelated families from different geographical origins with encephalopathy and hypopituitarism. Postings at GeneMatcher database and subsequent collaboration enabled independent discoveries to be merged and corroborated.[12] Patient 4 was mentioned in a synopsis about possible new candidate genes for autosomal recessive diseases before.[13] Written informed consent for exome sequencing and publication of medical histories and images was obtained by the parents of the patients and the family members investigated. Approvals from the corresponding ethical committee were obtained.

Genetic Analysis

Different NGS approaches have been used for exome sequencing (ES). Details to the methods used for exome sequencing of each patient are available upon reasonable request. ES in family-1: capturing: SureSelect Human All Exon 50 Mb kit (Agilent, Santa Clara, CA, USA); sequencing on a HiSeq 1500 (Illumina, San Diego, CA, USA), mapping (Human reference genome hg19) BWA-mem[14]; downstream processing: Samtools[15];

realignment around indels: GATK IndelRealigner[16]; detection of variants: VarScan2 [17].

ES in family-2: capturing: optimized SureSelect Human Exome kit (Agilent, Santa Clara, CA, USA); sequencing: HiSeq 2500 (Illumina); alignment: BWA[18]; downstream processing: Genome analysis (GATK), SAM and Picard Toolkits; calling of variants and indels: SAMtools (mpileup, bcftools, vcfutil); calling of substitution and variation: SAMtools pipeline (mpileup).

ES in family-3 was performed as described in Monies D et al. 2017.[13]

ES in family-4: trio exome sequencing of the index case and the parents as described in detail before by Kremer et al.[19,20];

ES in family-5 was performed through a commercial diagnostic laboratory (Sistemas Genómicos, S.L, Valencia, Spain); capturing: SureSelect Human All Exon v4; sequencing: on a HiSeq 2000 (Illumina); mapping: BWA aligner[18]; realignment: GATK pipeline; variant discovery: haplotype Caller tool and GATK[21]; annotation: ANNOVAR.[22]

ES in family-6 was performed as trio exome sequencing of the index case and the parents.

Postmortem Neuropathological Studies

Gross and histopathological analyses were performed in patient 1:III-3. Tissue samples were obtained from different areas of the CNS and the pituitary gland. Tissue from an age and gender matched child served as a control.

From all samples 3.0 μm thick paraffin sections were stained with hematoxylin and eosin (HE) Klüver Barrerea (KB). Immunohistochemical analysis was performed at paraffin sections from the pituitary gland using a Bench Mark XT automatic staining platform (Ventana, Heidelberg, Germany; ultraview Universal DAB detection kit) with the following primary antibodies: mouse anti-ACTH (Adrenocorticotrophic Hormone) (DAKO M3501 (02A39); 1:2000); mouse anti-FSH (Follicle Stimulating Hormone) (Zytomed 5063134 (SPM107); 1:2000), rabbit anti-HGH (Human Growth Hormone) (DCS G1100C002, 1:200), mouse anti-LH (Luteinizing Hormone), Zytomed 512-3094 (SPM103), 1:1500), mouse anti-Prolactin (Biogenix MU031-UC,1:300), mouse anti-TSH (Thyroid Stimulating Hormone) (Dako M3503 (0042), 1:500). From CNS sections, additional rabbit anti-GFAP (Glial Fibrillary Acidic Protein) (Dako, ZO334, 1:1000) staining was performed. Samples were examined at a Nikon Eclipse 80i equipped with a DISiF digital camera.

For immunofluorescence studies 4 μm thick paraffin sections were stained with primary polyclonal antibody Anti-HID1 (Sigma HPA031406; 1:100) and secondary antibody goat anti-rabbit Alexa Fluor 488 (1:200, Thermo Fisher Scientific). Sections were mounted with DAPI Fluoroshield (Abcam). Samples were examined at a Leica DM 2000 fluorescence microscope (Leica Microsystems, Wetzlar, Germany) at 620 × magnification equipped with a Leica DFC450C camera and Leica Application-Suite Version 4.7.

Cell Culture

Human skin fibroblasts from affected individuals (1:III-3, 4:II-2), heterozygous parents (1:II-1 and1:II-2) and unaffected controls were cultured in DMEM (Sigma-Aldrich, D5648) supplemented with sodium pyruvate, heat-inactivated 10% fetal calf serum and antibiotics. Before confluency, cells were passaged with a splitting ratio of 1:3; semiconfluent cultures at passages 4–10 were used for experiments. Cells were seeded onto 12-well plates containing a coverslip for immunofluorescence stainings.

Immunofluorescence Staining of Cultured Cells

Cells grown on coverslips were washed with warm PBS followed by incubations at room temperature with 4% paraformaldehyde in PBS for 20 minutes (fixation), 0.1% Triton X100 in PBS for 10 minutes (permeabilization), and 1% glycine in PBS for 10 minutes (reduction of background staining by binding of glycine to free aldehyde groups). Thereafter, blocking was done with 1% bovine serum albumin in PBS with 0.05% Tween 20 for 30 minutes. This blocking buffer was also used for the dilution of the primary and secondary antibodies. Cells were incubated with primary rabbit polyclonal anti-human HID1 antibody (Sigma, HPA031406, 1:100) and mouse monoclonal anti-58k Golgi protein antibody (Abcam, ab 27043, 1:200) for 1 hour, and with secondary donkey anti-rabbit IgG Alexa 488 antibody (ThermoFisher Scientific, A32790; 1:500) and horse anti-mouse IgG Texas Red antibody (Vector laboratories, TI-2000, 1:300) for 1 hour at room temperature. Next, coverslips were mounted onto glass slides in a mixture (4:1) of Mowiol® 4-88 mounting medium plus n-propylgallate as fading agent. Image acquisition was performed using a Leica confocal laser scanning microscope (Leica TCS SP5, setting: airy 1, average of 4 scans) and later modified by Adobe Photoshop® CS3.

Gene Expression Studies

Multiple sequence alignments: HID1 protein sequences of 87 species were identified searching the UniProt database (https://www.uniprot.org/). Multiple alignment was generated using MUSCLE.[23] BLASTP search for HID1 related proteins was performed online under standard conditions using Q8IV36 (UniProt) as input sequence against refseq_database human proteins.

In silico expression analysis of HID1: Gene expression data for human *HID1* transcript (Ensembl ID: ENSG00000167861.11, Gene ID: 283987) from 31 tissues published from the Genotype-Tissue Expression (GTEx) project (https://gtexportal.org/home/) were analyzed. Boxplots of the log2-transformed TPM ("Transcripts per Million") values were generated with help of R statistical software by using the graphical package ggplot2. Reordering of the categorical variables (factor levels) was performed with the forecast package. The data of the GTEx portal used for the analysis described in this manuscript were downloaded via "R2: Genomics Analysis and Visualization Platform (http://r2.amc.nl)" on 5 December 2018. The obtained dataset ("Normal Tissues GTEx v7 Prot_Coding-GTEx-11688-tpm-ensgtexv6") includes 11,688 samples, 53 tissues and 714 donors.

For analysis of *HID1* mRNA expression during human brain development we used data provided by the Allen Brain Atlas (BrainSpan Atlas of the Developing Human Brain) available at http://www.brainspan.org/rnaseq/search/index.html[24] and

a second dataset from Kang and colleagues.[25] Expression level of *HID1* in several human brain regions at different time points of fetal and postnatal ages were downloaded as RPKM (reads per kilobase of exon model per million mapped reads) and signal intensity values, respectively. In addition, RPKM values from Allen Brain Atlas of the fetal time points and the postnatal ages were analyzed separately for each brain region. Pearson's correlation analysis was used for calculation of the correlation coefficients and corresponding *P*-values of RPKM values or signal intensities, respectively, and ages.

RT-qPCR

Total RNA was extracted from unfixed tissue samples (patient 1: III-3 and a control) using the RNeasy Lipid Tissue-Kit (Qiagen, Hilden, Germany). DNAse treated total RNA was converted into cDNA (QuantiTec-Reverse-Transcription kit, Qiagen). Primers: HID1_foreward: 5'-CAGCTCACCACCAAGACGC-3', HID1_reverse: 5'-CTCAACGGCCTTGTAGCACA-3', EIF4_foreward: 5'-ATACGAGGCGCAAGGTG-3', EIF4_reverse: 5'-AC TTGTTGCACATCAATCCC-3', CYC1_foreward: 5'-AGTTTG ACGATGGCACCC-3', CYC1_reverse: 5'-GCCGCTTTATGG TGTAGAC-3'. Fluorescence data were compiled using the CFX384 qPCR system (BioRad, Hercules, CA, USA). Housekeeping genes *EIF4A2* and *CYC1* were co-analyzed for normalization of RNA content in each tissue sample.[26] Fold expression was calculated relative to HID1 expression in liver tissue of the control (qBase module, Bio-Rad CFX Manager V3.1.1517.0823).

Determination of the Extracellular Acidification Rate with the Seahorse XFe96 Analyzer

Primary human skin fibroblasts of affected individuals, heterozygous parents and four controls were cultured in 75 cm^2 flasks in DMEM (Sigma-Aldrich; D5648) to 80% confluency. Pheochromocytoma cells from the rat adrenal medulla (PC12 cells) carrying either wild-type or mutated HID1 gene[5] were cultured in DMEM (Sigma-Aldrich, D5468) supplemented with heat-inactivated 10% fetal calf serum, 5% horse serum, and antibiotics to 80% confluency. The medium was removed, and the cells were washed with 5 ml phosphate-buffered saline (PBS). The cells were detached with 0.05% trypsin/0.53 mM EDTA for 3 minutes. 3 ml of the cell suspension was added to 10 ml DMEM medium in a 15 ml tube. The cell suspension was centrifuged at 2,000 rpm for 5 minutes. The supernatant was discarded and the cell pellet was resuspended in 4 ml DMEM medium. For a 96-well plate, 12,000 cells per well were seeded. The plate was incubated for 1 hour under the lamina flow to allow the cells to attach. Plates were placed in the incubator at 37°C with 5% CO_2 overnight before measurement. The sensor cartridge was incubated with 200 µl XF Calibrant (Agilent Technologies, pH 7.4) per well at 37°C without CO_2 overnight. DMEM (Sigma-Aldrich; D5030) assay media was supplemented with 2 mM L-glutamine, 10 mM glucose, 1 mM sodium pyruvate and 15 mg/l phenol red. The pH was adjusted to 7.4. Prior to measurement DMEM medium of the seeded fibroblasts was discarded and the cells were washed two times with 120 µl assay medium. 180 µl of the seahorse medium was added and the

plate was incubated at 37°C without CO_2 for 1 hour. Potassium chloride (KCl) (225 mM, 450 mM and 900 mM) was also diluted in assay medium. 20 µl of KCl solutions were injected via the cartridge to reach final KCl concentrations of 22.5, 45 and 90 mM. The baseline measurement comprised 5 cycles, which include 3 minutes mixing, 2 minutes waiting and 3 minutes measuring for each cycle. After KCl injection, 8 measuring points were recorded, which also comprise 3 minutes mixing, 2 minutes waiting and 3 minutes measuring for each cycle. For statistical analysis of the KCl effect a parametric t-test was used. Baselined ECAR represents ECAR values normalized to the mean ECAR prior to KCl stimulation (time point 5). HID1 knockout in PC12 cells was described presiously.[5] For EACR assay, PC12 wild-type and HID1 knockout cells, 80,000 cells per well, were seeded on 96 well plates. According to the article of Hummer et al., 90 mM KCl was used for stimulation. The Seahorse measurement for PC12 cells was performed as described above for primary human skin fibroblasts.

Results

Description of Patients

The patients from families 1, 3, 4, 5 and 6 presented with epilepsy and muscular hypotonia during the neonatal period or within the first months of life, and none of them reached a psychomotor milestone such as turning, sitting or speaking. Moreover, two of them died within the first years of life due to respiratory complications or intractable seizures. One patient was affected less severely (2:IV-3). He learned to communicate without speech by using pictograms and gestures, and achieved walking with aid. All subjects manifesting early had various seizure types including generalized tonic clonic, myoclonic, complex-partial, tonic, and autonomic seizures. Notably, initial seizures were related to hypoglycemia in patient 3:IV-1. The EEG was characterized by generalized and/or focal slowing as well as multifocal sharp and poly sharp slow waves, evolving to hypsarrhythmia in some.

Cranial MRI displayed cerebral atrophy in patients 1:III-2 and 1:III-3, that was progressive in patient 1:III-3. Diffuse cerebral atrophy was also found in patient 5:II-1. The corpus callosum was thin on MRI images of patients 1:III-2, 1:III-3, 3:IV-1, 5:II-1 and 6:II-1. The pituitary glands appeared small in all patients, but no targeted investigations of the pituitary region were done (Fig 1). Clinical features are summarized in Table. Detailed case reports for all patients are given in Supplementary Table S1.

All patients developed clinical symptoms related to hypopituitarism and hormone deficiencies within the first months of life, prompting substitution with cortisone, desmopressin, somatotropic hormone, or thyroxine. Thyroid stimulating hormone (TSH) and peripheral thyroid hormones were diminished in all. No TSH increase upon
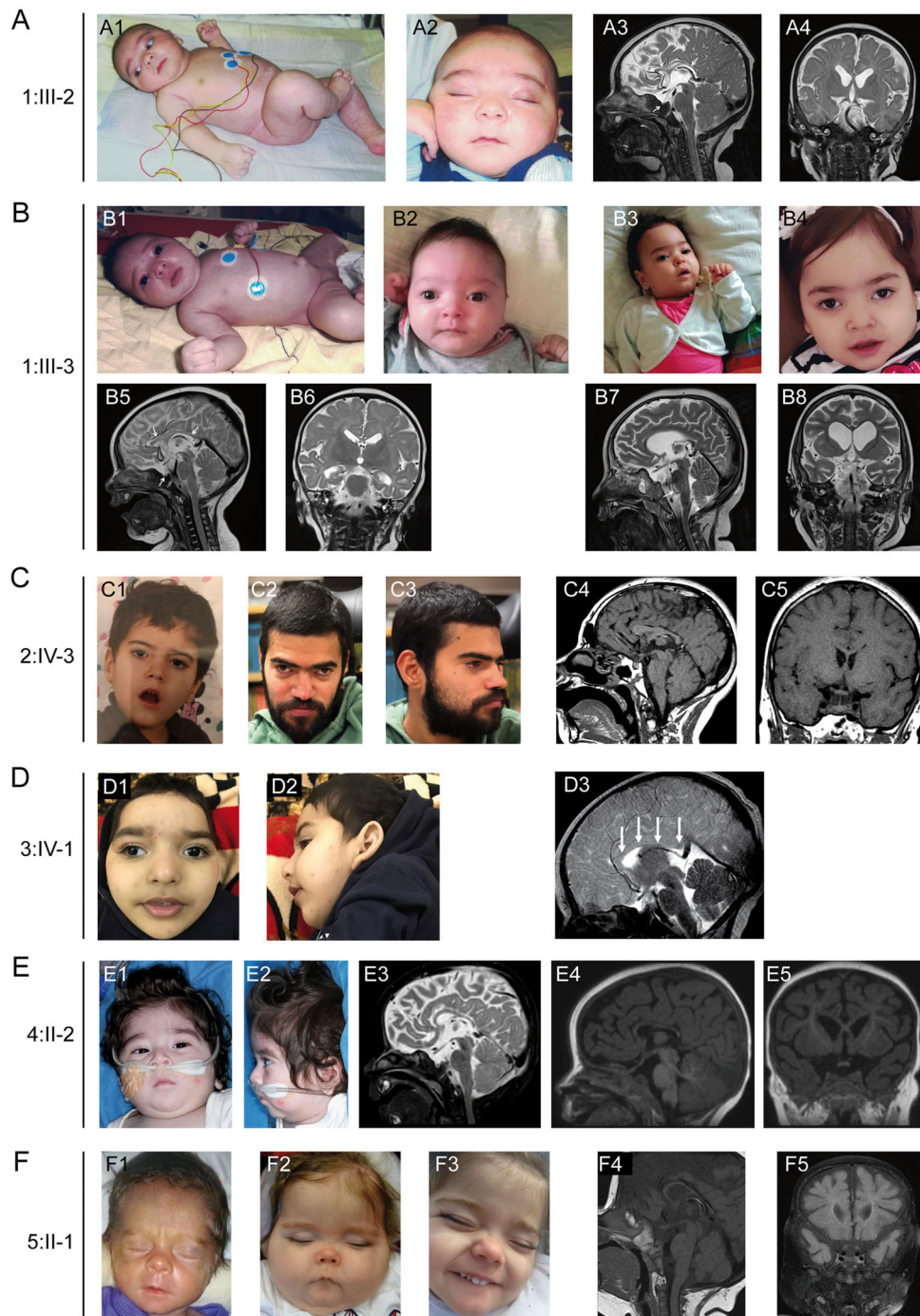
FIGURE 1: Clinical phenotype and MRI images of patients with bi-allelic HID1 variants. (A) Patient 1:III-2 at age 3 months (A1, A2). T2-weighted sagittal (A3) and coronal (A4) brain MR images at age 4 months indicate hypoplasia of the corpus callosum and a small sella turcica (white arrows). (B) Patient 1:III-3 at age 2 months (B1, B2), at age 2 years (B3), and at age 3 years (B4). T2-weighted sagittal and coronal brain MR images age 4 months (B5, B6) and at age 3 years and 2 months (B7, B8) show a relatively small pituitary gland and a thin and dysplastic corpus callosum (B5 white arrows). Note also distinct cortical atrophy and enlargement of the inner ventricles evolving during the course of disease (B7, B8). An unspecific signal alteration of the ventral part of the pons (B7, white arrow) is also marked. (C) Patient 2:IV-3 at age 3 years (C1) and at age 21 years (C2, C3). T1-weighted brain MR image displays a relatively small pituitary gland and a small corpus callosum. No generalized brain atrophy is visible. (D) Patient 3:IV-1 at age 3 years (D1, D2). T2-weighted brain MR image displays a thin corpus callosum (D3, white arrows). (E) Patient 4:II-2 at age 8 months (E1, E2), T2 (E3). T1-weighted (E4) sagittal brain MR images show a thin corpus callosum. T1-weighted coronal image depicts enlarged lateral ventricles and suggests gyral atrophy (F) Patient 5:II-1 at age 2 weeks (F1), at age 20 months with *cushingoid* face (F2) and at age 3 years (F3). Sagittal T1-weighted MR image at age 18 months indicates a dysplastic corpus callosum and a small pituitary gland (F4), while a coronal FLAIR image depicts mild gyral atrophy (F5). Consent was obtained from parents/legal guardians for use of clinical photographs shown in this Figure (including parental consent for inclusion of the identifiable (non-obscured) facial photographs).

TABLE. Clinical Characteristics of Patients with Biallelic *HID1*-Mutation

	Family 1	Family 1	Family 2	Family 3	Family 4	Family 5	Family 6
	Propositus 1	Propositus 2	Propositus 3	Propositus 4	Propositus 5	Propositus 6	Propositus 7
	1:III-2	1:III-3	2:IV-3	3:IV-1	4:II-2	5:II-1	6:II-1
Origin/Ancestry	Turkey	Turkey	Tunisia	Saudi Arabia	Turkey	Spain	Pakistan
Gender	Male	Female	Male	Male	Female	Female	Male
HID1 variants (NM_030630.2)	c.1297C>T c.1297C>T	c.1297C>T c.1297C>T	c.388C>T c.1598T>C	c.2318dupC c.2318dupC	c.1297C>T c.1297C>T	c.1149 + 1G>T c.81_83delinsTT	c.560G>A c.560G>A
HID1 variants (protein)	p.Arg433Trp p.Arg433Trp	p.Arg433Trp p.Arg433Trp	p.Gln130[a] p.Leu533Pro	p.Val774Cysfs*11 p.Val774Cysfs*11	p.Arg433Trp p.Arg433Trp	splice-site (ex 9_10) p.Asp28Lfs*68	p.Gly187Asp p.Gly187Asp
Gestational age	41 weeks	39 weeks	40 weeks	40 weeks	39 weeks	31 + 5 weeks	32 weeks
Birth weight[a]	3,830 g (54P., 0.09z)	3,130 g (41P., −0.23z)	2,880 g (13P., −1.15z)	3,000 g (10P., −1.26z)	3,560 g (74P., 0.63z)	1,130 g (9P., −1.36z)	1,500 g (21P., −0.71z)
Birth length[a]	55 cm (91P., 1.34z)	50 cm (58P., 0.2z)	51 cm (60P., 0.25)	*NA*	48 cm (25P., −0.66z)	35 cm (<1P., −2.22z)	*NA*
Birth head circumference[a]	36 cm (63P., 0.32z)	35 cm (73P., 0.6z)	34 cm (31P., −0.51z)	*NA*	34.5 cm (59P., 0.24z)	*NA*	<1P.
Age at last follow up	3 months	3 years	24 years	2 years	21 months	4 years	4 years
Weight[b]	4,530 g (<1P.,-2.85z)	17 kg (94P., 1.55z)	39 kg (<1P., −4.88z)	11 kg (19P., −0.89z)	11.5 kg (49P., 0.03z)	11 kg (<1P., −3.43z)	13.6 kg (8P., −1,43z)
Height[b]	55 cm (<1P.,-3.17z)	96 cm (66P., 0.42z)	160 cm (<1P., −2.31z)	77.5 cm (1P., −2.63z)	75 cm (<1P., −2.82z)	77 cm (<1P., −6.03z)	*NA*
Head circumference[b]	37 cm (<1P., −2,99z)	44 cm (<1P., −2.78z)	51 cm (<1P., *NA*)	42 cm (<1P., −3.77z)	44 cm (<1P., −3.43z)	43 cm (<1P., *NA*)	42 cm (<0.4P., *NA*)
Current Status	died (age 1 year)	died (age 3 years)	alive	died (age 2 years)	alive	alive	alive
Morphology							
Hypertelorism	+	+	−	+	−	−	NA
Synophris	+	+	+	Mild	Mild	Mild	NA
Long eyelashes	+	+	−	+	+	+	NA
Hypertrichosis	NA	NA	−	−	+	−	+
Neurology							
Motor development	Absent	Absent	Delayed	Absent	Absent	Severe delay	Absent
Language	*NA*	No speech	No speech, uses pictograms to communicate	No speech	No speech	No speech	No speech
Seizures	+	+	−	+	+	+	+
Seizure quality	GTCS, TS, MS, AS, CPA, HS	GTCS, TS, MS, AS, CPA, HS	−	MS, GTCS, HS	GTCS, CPS	MS, GTCS	GTCS, HA, HA, TS, CPS
EEG-findings	GS, FS, FSW, hypsarrhythmia	GS, FS, FSW, hypsarrhythmia	normal	GS, FSW	GS, FSW	GS, FSW	GS, FSW
Muscular hypotonia	+	+	−	+	+	+	+
Spasticity	−	−	+	*NA*	+	+/−	−
Nystagmus	+	+	−	*NA*	−	−	−
Fixation	−	−	+	−	−	−	−
Eye	Retinal dystrophy	−	−	−	*Strabism*	−	−
Brain MRI							
Corpus callosum	Thin	Thin	Normal	Thin	Thin	Thin	Thin
Pituary gland	Small	Small	Small posterior lobe	Small	Normal	Small anterior pituitary, absence of posterior lobe	Small
Brain atrophy	−	Progressive	−	−	Progressive	Progressive	Progressive

[a]Centiles according to *Fenton TR, Kim JH. BMC Pediatr. 2013; 13:59.*

[b]Centiles according to *Centers for Disease Control and Prevention, National Center for Health Statistics. CDC growth charts: United States.* http://www.cdc.gov/growthcharts/.

AS = Autonomic Seizures; CPS = Complex-Partial Seizures; FS = focal slowing; FSW = focal/multifocal sharp slow waves; GS = generalized slowing; GTCS = Generalized Tonic Clonic Seizures; HA = hypsarrhythmia; HS = Hypoglycemic Seizures; MS = Myoclonic Seizures; NA = not applicable; nd = not done; TS = Tonic Seizures.

stimulation with TSH-releasing hormone was found in patient 1:III-2. Hypoglycemia suggesting growth hormone deficiency and/or cortisol deficiency was noticed in patients 3:IV-1, 4:II-2, 5:II-1, and 6:II-2. Low somatotropic hormone values, and inadequately low cortisol levels at least during fever or infection were observed in 1:III-2 and 1:III-3. An inadequate increase of antidiuretic hormone during a fluid deprivation test in patient 1:III-2 indicated involvement of the posterior pituitary gland. Endocrine data of all patients are summarized in Supplementary Table S2 and the detailed endocrine values obtained during the course of disease for patient 1:III-2 are depicted in Supplementary Table S3.

Similarities of the facial gestalt included marked eyebrows with a discrete form of synophris, long eyelashes and mild hypertelorism. Male patients 1:III-2 and 3:IV-1 had ambiguous genitalia such as micropenis and cryptorchidism, accompanied by hypospadia and phimosis in patient 1:III-2. Cryptorchidism was reported in patient 6:II-1 as well.

Genetic Analysis

Variants in *HID1* (NM_030630; ENST00000425042.2) were c.1297C>T (p.R433W) in family-1 and family-4, c.388C>T (p.Q130*) and c.1598T>C (p.L533P) in family-2, c.2318dupC (p.V774C*fs**11) in family-3, c.1149 + 1G>T and c.81_83delinsTT (p.D28L*fs**68del) in family-5 and c.560G>A (p.G187D) in family-6. An extensive segregation analysis was performed in family-1 (Fig 2A). Interestingly, patient 2:IV-3 carried the missense variant p.L533P in compound-heterozygous state together with a nonsense variant, even though the parents were consanguineous. Only affected individuals carried biallelic variants.

A search of the Genome Aggregation Database (gnomAD) revealed one heterozygous match for the c.1297C>T (p.R433W) variant (allele frequency 0.000004345). No match was found for variants c.1598T>C (p.L533P) and c.560G>A (pG187D) (search date: April, 7th, 2021). All missense variants were predicted to be disease causing by Mutation-Taster[27] (score 0.999) and PolyPhen[28] (score 1.0). PROVEAN[29] scores were −7.49 (deleterious) for p.R433W, −6.817 (deleterious) for p.L533P and −6.28 for pG187D. SIFT[30] predicted variants as damaging. Variant effect prediction (VEP) by ENSEMBL[31] was "IMPACT = MODERATE" for all variants. Although HID1 is a candidate gene, we applied the same ACMG guidelines validated for genes with established gene-disease association. Missense variants were classified to be "likely pathogenic" according to standard criteria of the American College of Medical Genetics (ACMG),[32] that is absence in population databases

(PM2), allelic data (PM3), computational and predictive data (PP3) and segregation data in a recessive trait (PP1) supports the classification of a moderate (PM) to strong (PS) pathogenicity for all variants. Variants c.2318dupC and c.81_83delinsTT cause frameshifts and lead to premature STOP codons.

The positions of all variants in the *HID1*-gene are shown in Fig 2B.

Searching the UniProt database we identified proteins in 87 species with high similarity to human HID1. Multiple alignment of protein sequences identified large parts of the HID1 protein to be highly conserved throughout evolution (not shown). Missense variants identified in families 1, 2, 4 and 6 affect amino acids which are widely conserved in taxonomic lineages from hominidae down to nematoda (Fig 2C). In a BLASTP search for human proteins related to HID1 only dymeclin (DYM) was found to match significantly over a region of about 231 amino acids. This region spans HID1 amino acids from 373 to 569. Thus, missense variants p.R433W and p.L533P lie within this region of highest similarity.

Postmortem Findings

The family of propositus 1:III-3 agreed on autopsy after the girl had died during pneumonia at the age of 3 years and 7 months. Macroscopic examination demonstrated severe brain atrophy with 702 grams weight in total (age related normal value 1200 grams), enlarged lateral ventricles and a thin corpus callosum (Fig 3A). Histological examination of the frontal cortex and cerebellum displayed normal distribution of neurons. In the Kluver Barrera staining the myelination of the axons appeared normal. With antibodies against GFAP activated astrocytes are shown mainly in the cerebral cortical areas and less in the cerebellum (Fig 3B). Histological analysis of brainstem, basal ganglia and hippocampus did not show any specific pathology (not shown). The pituitary gland showed a normal adenoid histology, but immunohistochemical staining disclosed distinct reductions of FSH, HGH, LH, prolactin and TSH whereas ACTH was only moderately reduced compared to the control (Fig 4A). Immunofluorescence staining with antibodies against HID1 protein showed a cytoplasmic expression in the neuronal cells of the frontal cortex, the cerebellum, and in the adenoid cells of the pituitary gland in the patient and the control (Fig 4B).

Gene Expression Analysis

In silico analyses of the HID1 transcript expression showed highest expression levels in several brain regions and different secretory tissues that is pancreas, salivary gland, prostate and particularly pituitary gland (Fig 5A). Analyzing HID1 mRNA expression during human brain
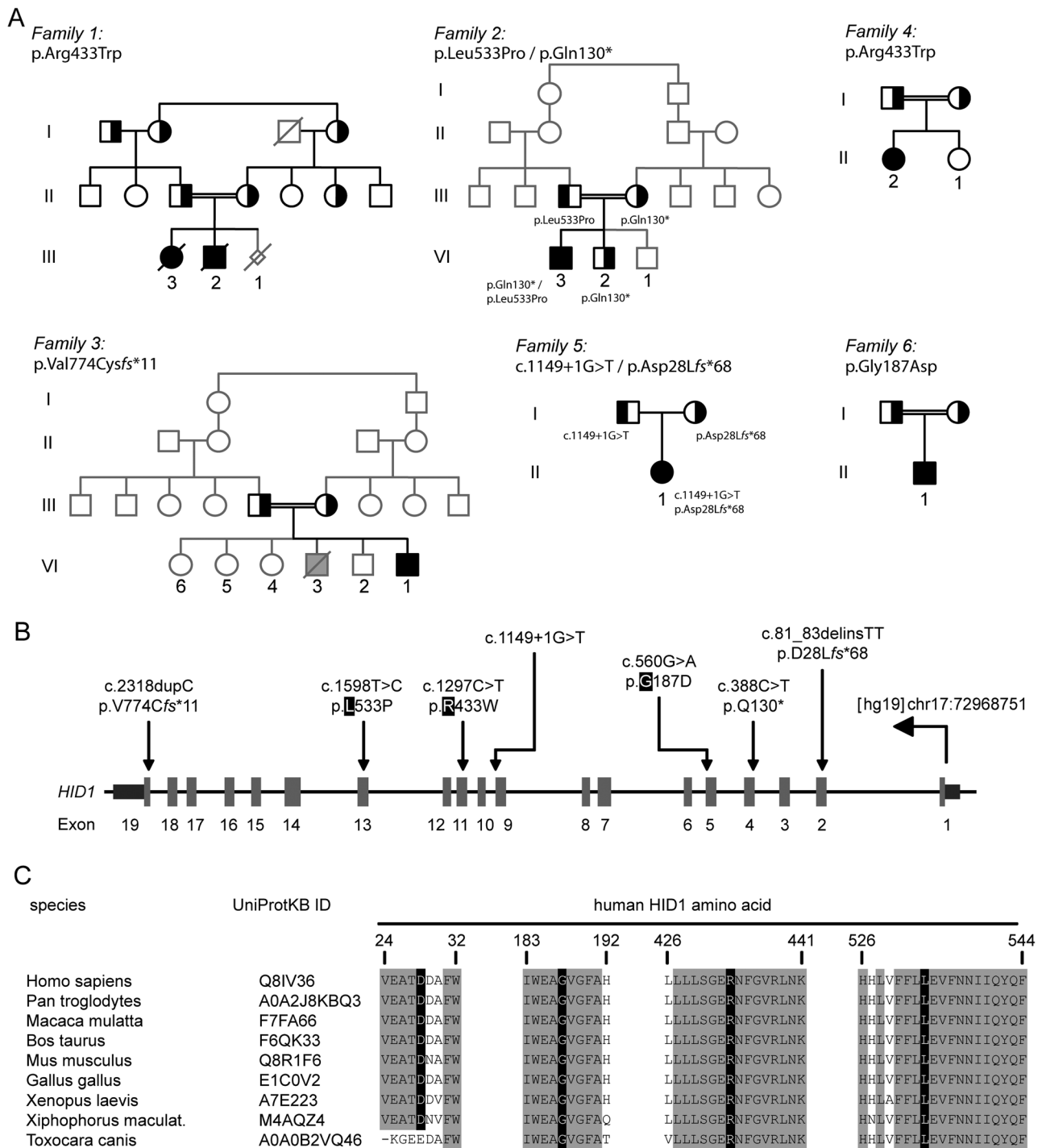
A

B

C

FIGURE 2: *HID1* variants. (A) Pedigrees of families 1 to 5. Family members who underwent genetic testing for the respective HID1 variants are indicated with black and white symbols. Grey-and-white symbols correspond to family members not tested for the familial *HID1* variant. (B) The human *HID1* gene (NM_030630) consists of 19 exons on the minus strand of chromosome 17 (hg19 coordinates: chr17:72946837–72968854). *HID1* variants found in the families reported are highlighted. Missense variants are indicated white with black background. (C) Alignment of the protein sequences in vicinity to amino acids D28, R433 and L533, between human and homologous HID1 proteins. R433, L533 and adjacent amino acids are widely conserved between species, D28 is also highly conserved except for nematoda.

development by using the data of the Allen brain atlas[24] and of Kang and colleagues[25] showed that HID1 expression significantly increased with gestational age averaged over all CNS regions (Fig 5B, C). This correlation was also found in almost all regions of the human brain, when analyzed separately (not shown). No further significant elevation of HID1 expression was found after birth (not shown).
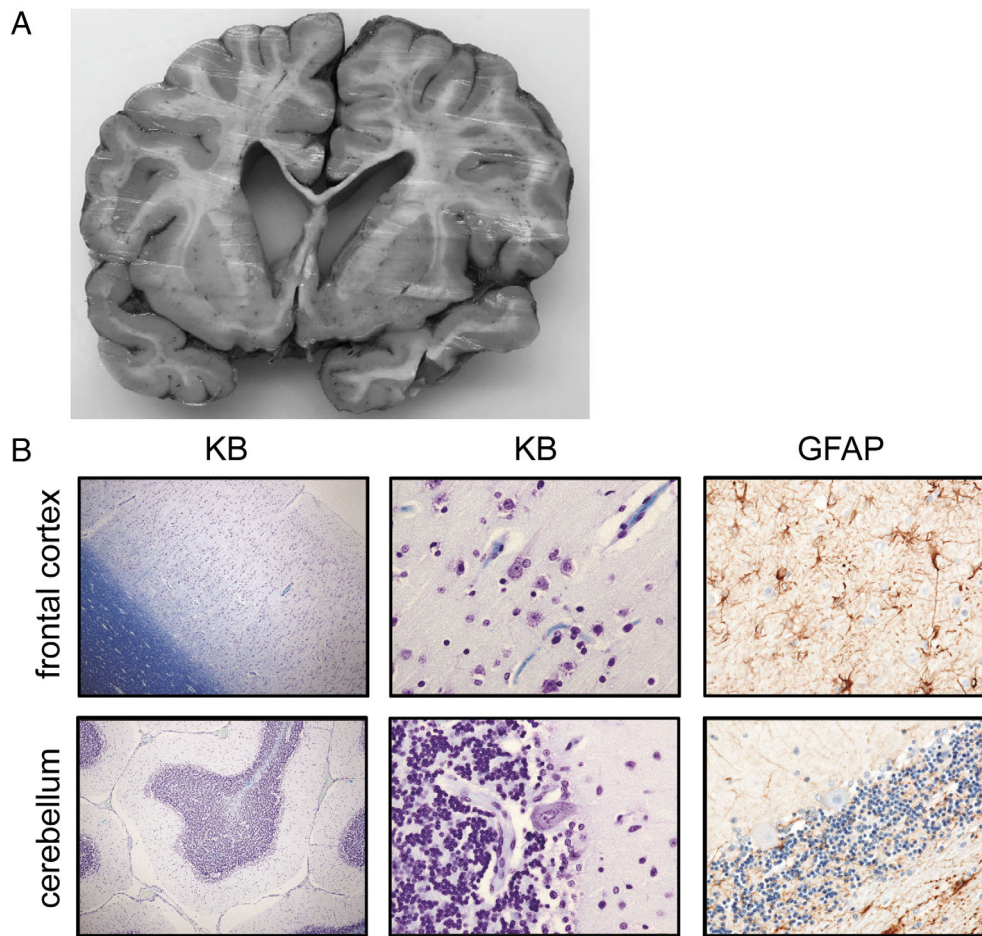
FIGURE 3: Neuropathological findings of patient 1:III-3. (A) Gross examination of a coronal brain section of patient 1:III-3 at age 3 years shows cerebral atrophy (brain weight 702 g), enlargement of the lateral ventricles and a thin corpus callosum. The cortical grey matter is well distinguished from the white matter. (B) Klüver Barrera (KB) staining displays normal cortical architecture in the frontal cortex and cerebellum, and no signs of de- or hypomyelination (magnification ×40 1st column; ×400 2nd column). Activated glial cells are numerous in frontal cortex as confirmed with antibodies against GFAP (magnification ×400).

In line with the results of computational analysis of public GTEx data, determining the level of *HID1* transcription by reverse transcription qPCR in *post mortem* brain tissue of patient 1:III-3 and the control displayed a higher HID1 expression in cerebellum (CB), anterior frontal cortex (Cf) and striatum (Str) when compared to liver (Fig 5D). Expression in different tissues was lower in patient 1:III-3 compared to control except for Cf.

Immunofluorescence Staining of Cultured Fibroblast Cells

Immunofluorescence staining of cultures fibroblast showed a clear co-localization of HID1 and Golgi marker 58 K in heterozygous HID1 variant family members (1:II-1 B1-B3; 1:II-2 C1-C3), bi-allelic HID1 variant patients (1: III-3 (D1-D3, 4:II-2 E1-E3), and a control (Ctrl, A1-A3). No differences with regard to degree of HID1 expression and expression pattern were detected between controls

and individuals with single-allelic or bi-allelic HID1 variants (Fig 6).

Extracellular Acidification

We determined the relative change of the extracellular pH close to the cell surface upon KCl stimulation in patient fibroblasts (1:III-3 and 4:II-2) versus controls and in PC12 wild-type versus *HID1*-knockout cells as a marker for TGN acidification. The extracellular acidification rate (ECAR) was measured with the Seahorse XFe96 analyzer. ECAR represents changes in pH at the cellular surface over time (mpH/min) upon KCl induced TGN vesicle fusion. The optimal dose of KCl was determined in patient 4:II-2 and controls. No effect was visible with 22.5 mM KCl (Fig 7A). 90 mM KCl showed the most pronounced effect on the ECAR, but also highest standard deviations. Therefore, 45 mM KCl was selected for further experiments. Baseline ECAR and stimulated ECAR after administration of 45 mM
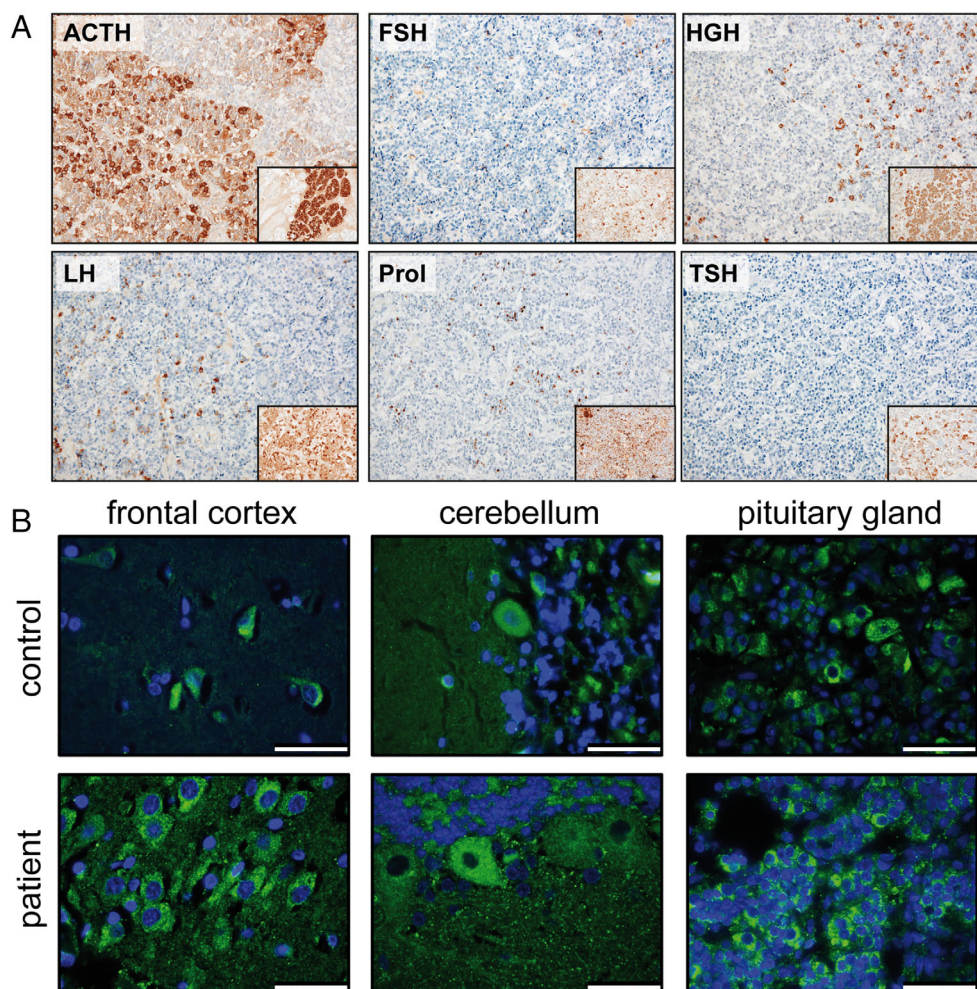
FIGURE 4: Pituitary Gland. (A) Analysis of the pituitary gland of patient 1:III-3 shows normal adenoid morphology. Staining with antibodies against pituitary hormones depicts moderate ACTH reduction, while FSH, HGH, LH, Prolactin (Prol) and TSH are strongly reduced compared to the control (inlay) (magnification 200×). (B) Immunofluorescence analysis with antibodies against HID1 shows a cytoplasmic expression in neuronal cells of the frontal cortex and cerebellum and in adenoid cells of the pituitary gland in patient and control (magnification ×630, white bars correspond 50 μm).

KCl were determined (Fig 7B, D). To better visualize the results, data have been merged into the baselined ECAR (Fig. 7C, E). Therefore, the measuring point prior to KCl administration was set to 100% for each sample. The relative change in ECAR from the baseline measuring point to the stimulated time point was analyzed (Fig. 7C, E). The increase of the baselined ECAR upon KCl stimulation was found to be significantly lower in fibroblasts of both affected individuals compared to controls and heterozygous parents (1:II-1; 1:II-2) of individual 1:III-3 (Fig. 7C, E).

To prove that the results obtained by this method really reflect hampered TGN function due to biallelic HID1 mutations, we additionally determined the ECAR in PC12 wild-type and PC12 *HID1*-knockout cells. In accordance with our results, this experiment also showed a significantly lowered ECAR upon KCl stimulation PC12 *HID1*-knockout cells (Fig. 7F, G).

Discussion

In this study, we identified biallelic mutations in *HID1* as a novel cause for an epileptic encephalopathy with hypopituitarism as the leading presentation in seven patients from six unrelated families. All patients shared comparable findings at brain imaging, including mild to moderate cerebral atrophy and a thin corpus callosum. In six of them epilepsy was severe and intractable despite the use of multiple antiepileptic drugs. Pituitary gland hormones were altered in all patients, but were not assessed in a comprehensive and standardized manner. However, hypopituitarism was diagnosed in all between 2 and 6 months of age (mean 3 months) and every patient was in need of substitution of one or more hormones.

Postmortem neuropathological findings in patient 1: III-3 confirmed a cerebral atrophy with severely reduced brain weight, enlarged ventricles and thin corpus callosum.
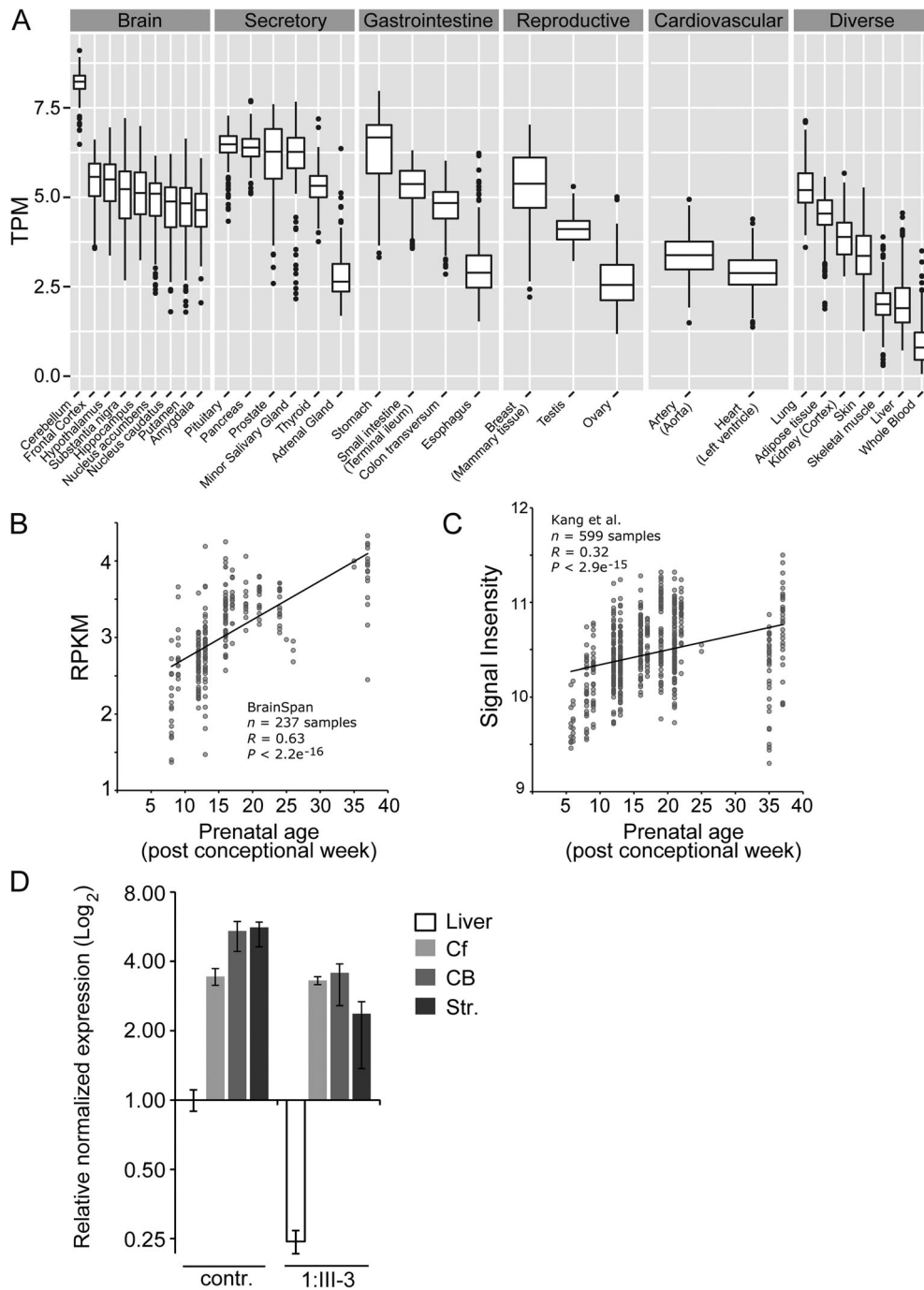
FIGURE 5: HID1 expression. (A) Expression of HID1 transcript in different human tissues. Data from the Genotype-Tissue Expression (GTEx) Project were downloaded from the R2: Genomics Analysis and Visualization Platform. Gene and transcript expression are shown in transcripts per million (TPM) (for calculation see methods section). HID1 is highly expressed in different parts of the brain, with highest expression in cerebellum. High expression levels are found in most of the secretory tissues also, with highest expression in the pituitary gland and the pancreas. Boxplots of log2-transformed TPM values for HID1. The boxplots of each category "BRAIN", "SECRETORY TISSUES", "GI", "REPRODUCTIVE", "CARDIOVASCULAR" and "DIVERSE" are sorted by their median values in descending order. (B, C) Expression level of *HID1* in human brain (merged data of different brain regions). Data at different time points of fetal ages were downloaded as RPKM (reads per kilobase of exon model per million mapped reads) values (BrainSpan) or signal intensities (Kang et al.) respectively. Expression values of HID1 at different weeks *post-conceptionem* were analyzed. Pearson's correlation analysis was used for calculation of the correlation coefficients and corresponding *P*-values of RPKM values or signal intensities respectively and ages. (D) Compared to an age matched control HID1 mRNA expression is lower in liver tissue and two brain regions (CB and Str) in patient 1:III-3. Fold expression was calculated with the integrated qBase module of the Bio-Rad CFX Manager 3.1 (3.1.1517.0823) software. For comparison of data from only one patient with one control, statistical significance was not calculated. qPCR experiments were done in triplicate.
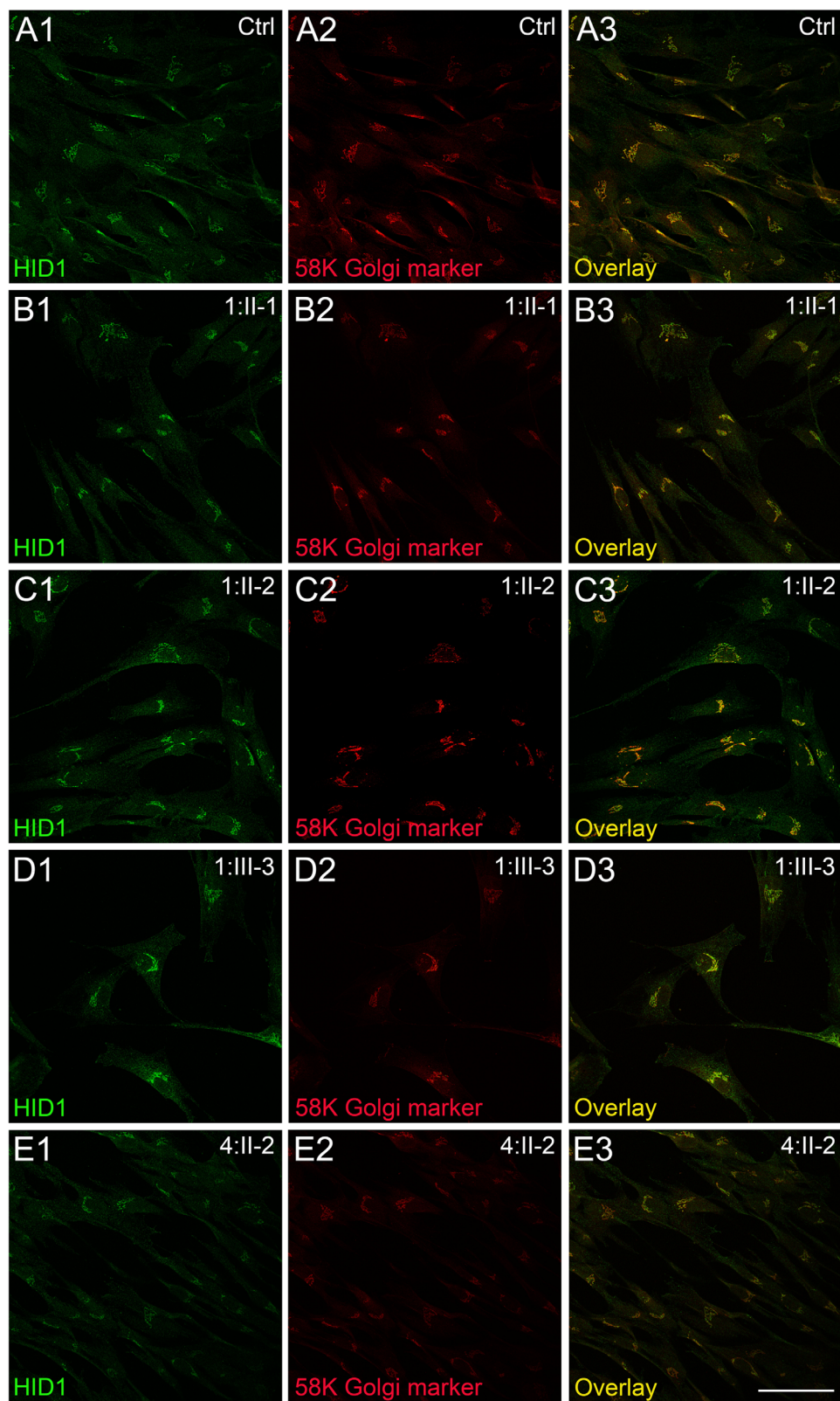
FIGURE 6: HID1 and Golgi staining of fibroblasts. Double immunofluorescence staining of cultured fibroblast cells from patients and family members in comparison to a control patient. Representative confocal micrographs of a control individual (Ctrl, A1–A3), single-allelic HID1 variant family members (family-1,1:II-1; B1–B3; 1:II-2, C1–C3), and bi-allelic HID1 variant patients 1:III-3 (D1–D3) and 4:II-2 (E1–E3) stained with rabbit polyclonal antibodies against human HID1 (green) and mouse monoclonal antibodies against 58K Golgi marker (red). The overlay (yellow) shows a co-localization of HID1 and the Golgi apparatus in all fibroblasts. Scale bar = 35 μm.
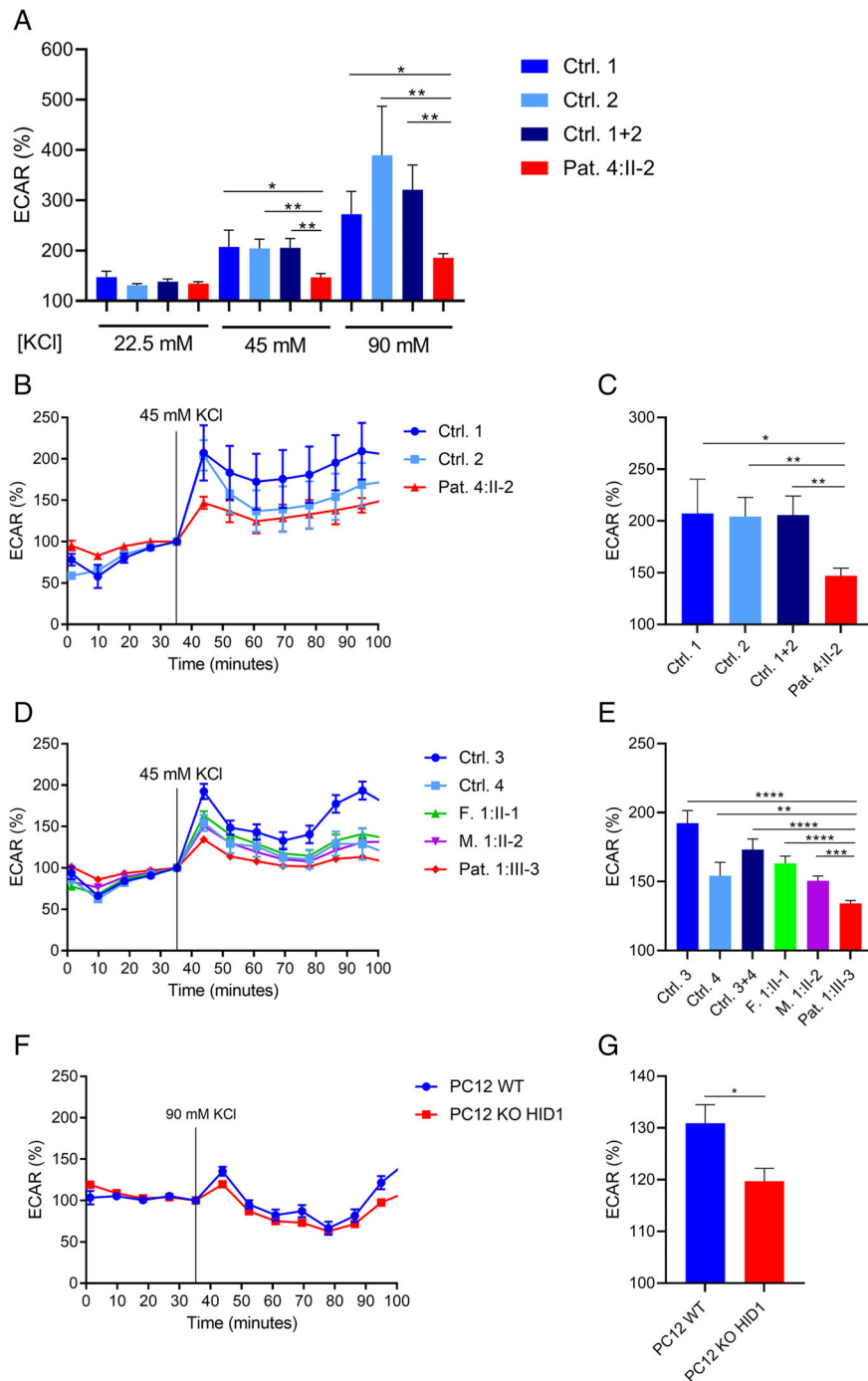
FIGURE 7: Extracellular acidification rate (ECAR) dependent on HID1 function. (A) Analysis of the mean relative ECAR change demonstrates that addition of 22.5 mM KCl was not sufficient to induce a significant increase of ECAR in any individual, while addition of 45 and 90 mM KCl induced a significantly higher increase in controls than in the affected individual 4:II-2. A parametric t-test was used to analyze the differences between the affected individuals and controls. Mean ± SEM are shown. *$p < 0.05$; **$p < 0.01$. (B–G) Baseline ECAR and relative change in (ECAR) in fibroblasts and PC12 cells after addition of potassium chloride (KCl). (B) Analysis of the relative change in ECAR over time shows lower values at all time points after addition of 45 mM KCl for the affected bi-allelic individual (4:II-2; n = 16 wells) compared to two controls (each n = 8 wells). (C) Analysis of the mean relative change of ECAR directly after 45 mM KCl addition reveals a significantly lower value in patient 4:II-2 compared to controls (time point 6 compared to time point 5). (D) Relative change in ECAR in the affected bi-allelic individual (1:III-3; n = 32 wells), heterozygous parents (father 1:II-1; n = 16 wells and mother 1:II-2; n = 16 wells) and two controls (each n = 14 wells) over time. (E) Mean relative change directly after 45 mM KCl addition is significantly lower in 1:III-3 compared to controls and heterozygous parents (time point 6 compared to time point 5). (F) Relative change in ECAR in PC12 wild-type and HID1 knockout cells over time. (G) Mean relative change directly after 90 mM KCl addition is significantly lower in HID1-knockout compared to wild-type cells (time point 6 compared to time point 5). A parametric t-test was used to analyze the differences between the affected individuals and controls. Mean ± SEM are shown. *$p < 0.05$; **$p < 0.01$; ***$p < 0.001$; ****$p < 0.0001$.

The macroscopic morphology of other brain areas appeared normal. Microscopic examination revealed neither axonal demyelination nor signs for abnormal neuronal cortical migration.

In line with the clinical findings of hypopituitarism, staining intensities with antibodies against pituitary hormones were substantially reduced, whereas HID1 staining of the adenoid cells of the anterior pituitary gland was not. Additionally, analysis of HID1 transcript expression, limited by comparing only one patient and a single control, did not indicate a substantial decrease in HID1 expression in three CNS regions.

It has been shown that HID1 is involved in vesicle formation and protein processing at the TGN[3,4,33] and that loss of HID1 function impairs TGN function.[5] As expected from these studies, we found HID1 to be localized to the TGN in fibroblasts from different wild-type controls and heterozygous parents of family-1 (1:II-1, 1:II-2). No differences with regard to localization and staining were found in fibroblasts from two HID1 patients with the missense mutation p.R433W (1:III-3 and 4:II-2). Collectively, these findings did not demonstrate definitely that HID1 mutations caused CNS pathology in our patients but were compatible with the hypothesis that *HID1* missense mutations lead to impaired HID1 function at the TGN rather than to HID1 protein loss in neuronal and secretory cells of the brain. In order to prove that the *HID1* missense mutation p.R433W hampers TGN function we performed further experiments.

The Golgi function is directly dependent on a successive luminal acidification, generated mainly by a vacuolar H + ATPase (V-ATPase) and a faulty regulation of Golgi pH leads to defects in protein glycosylation (reviewed in[34]). From the endoplasmic reticulum (ER) to the secretory vesicles, the luminal pH constantly decreases during the sorting processes within the TGN. This TGN acidification is the reason for a subsequent extracellular acidification upon vesicle release.[35] Hummer et al. evaluated this process in PC12 *HID1* knockout cells. They found a defective TGN acidification after potassium chloride stimulation that impairs the formation of large dense core vesicles (LDCV) and describe this as causative for a misrouting of hormones to the lysosome with subsequent degradation.[5] In this study we found that, in addition to the decrease in TGN acidification, the extracellular acidification rate (ECAR) is concomitantly reduced in PC12 *HID1* knockout cells.

We applied the same assay for quantitative ECAR analysis of fibroblasts from two of our patients to depict impaired HID1 function and found a significant lower baselined ECAR increase in response to KCl treatment compared to wild-type controls and heterozygous parents. Thus, in line with previously published data from PC12 cells[5] this demonstrates disturbed TNG function in primary cells of patients with biallelic *HID1* variants.

In this first cohort of patients with a HID1 related syndrome, we did not find any correlation between type or location of genetic variants and clinical phenotype. Variants were identified throughout the entire gene without hint for a critical functional domain. Missense variant p.R433W and nonsense variant p.V774Cfs*11 led to a comparable severe phenotype, whereas the by far less affected patient 2:IV-3 carries a nonsense and a missense variant in compound heterozygous state. Interestingly, missense variant p.R433W was identified independently in family 1 and family 4, respectively. No direct relationship between the families is known, but both come from a region in the southwest of Turkey (near the city Kahramanmaras), suggesting that this variant could be a founder mutation.

Highly conserved homologous *HID1*-genes have been identified in several species. Data from different expression studies indicate the relevance of *HID1* for neuronal and secretory cell function and the development of the brain, supporting the concept that impaired HID1 function during fetal brain development refers to the phenotype of early infantile encephalopathy, as seen in most of our patients.

Over a segment of about 196 amino acids HID1 shows sequence similarity to Dymeclin (DYM) (HID1 amino acid 373 to 569, alignment score 40–50). Two different forms of syndromic osteochondrodysplasia are associated with biallelic mutations in *DYM*. SMC1 is characterized by a mainly skeletal phenotype, whereas patients with DMC additionally exhibit a neuropathological phenotype.[2,10,11] Interestingly, there is mentionable overlap of HID1 and DYM protein function and the neuropathological phenotypes associated with dysfunction of the proteins. Like in HID1 deficient patients, microcephaly, corpus callosum hypoplasia and mild to severe intellectual disability can be found in DMC. Like HID1, DYM comprises a myristoylation domain, binds to the TGN[36,37] and defective DMY leads to disturbance of TGN function.[38,39] In contrast to HID1, DYM is strongly expressed in fibroblasts, skeletal muscle and cartilage tissue[39] attaining a link to the skeletal phenotype in SMC and DMC.

In summary, we provide evidence that bi-allelic mutations in *HID1* in six children and a young man from six unrelated families cause a syndrome with a characteristic infantile onset phenotype encompassing encephalopathy, corpus callosum hypoplasia, hypopituitarism, epilepsy, visual impairment and severe developmental

delay as the main clinical signs. Our findings add mutations in *HID1* as an underlying pathology to the group of syndromic encephalopathies caused by hampered TGN functions. Further functional studies and knockout models are required to test in detail how impairment of HID1 function during fetal brain development contributes to the phenotype of our patients.

Acknowledgments

Author Contributions

A.S., A.W., R.G.F. and A.H. contributed to the conception and design of the study; A.H., A.S., A.M., L.H., M.A., B.A., B.H., C.A., S.B.W., H.A., S.R.S., A.R., B.A.N., C.B., P.G., S.V., S.K.B., T.H., E.G., J.P.S., S.E., K.L.S., M.D.A., T.A., D.T., W.W., M.A., R.G.F., J.A.M. and A.W. contributed to the acquisition and analysis of data; A.W., A.S., J.A.M., R.G.F., C.B., F.S.A. and A.H. contributed to drafting the text and preparing the figures.

Potential Conflicts of Interests

Nothing to report.

References

1. de Matteis MA, Luini A. Exiting the Golgi complex. Nat Rev Mol Cell Biol 2008;9:273–284.

2. Ailion M, Thomas JH. Isolation and characterization of high-temperature-induced Dauer formation mutants in *Caenorhabditis elegans.* Genetics 2003;165:127–144.

3. Mesa R, Luo S, Hoover CM, et al. HID-1, a new component of the peptidergic signaling pathway. Genetics 2011;187:467–483.

4. Wang L, Zhan Y, Song E, et al. HID-1 is a peripheral membrane protein primarily associated with the medial- and trans- Golgi apparatus. Protein Cell 2011;2:74–85.

5. Hummer BH, de Leeuw NF, Burns C, et al. HID-1 controls formation of large dense core vesicles by influencing cargo sorting and trans-Golgi network acidification. Mol Biol Cell 2017;28:3870–3880.

6. Saitsu H, Kato M, Mizuguchi T, et al. De novo mutations in the gene encoding STXBP1 (MUNC18-1) cause early infantile epileptic encephalopathy. Nat Genet 2008;40:782–788.

7. Borck G, Wunram H, Steiert A, et al. A homozygous RAB3GAP2 mutation causes Warburg micro syndrome. Hum Genet 2011;129:45–50.

8. Handley MT, Morris-Rosendahl DJ, Brown S, et al. Mutation spectrum in RAB3GAP1, RAB3GAP2, and RAB18 and genotype-phenotype correlations in Warburg micro syndrome and Martsolf syndrome. Hum Mutat 2013;34:686–696.

9. Alshammari MJ, Al-Otaibi L, Alkuraya FS. Mutation in RAB33B, which encodes a regulator of retrograde Golgi transport, defines a second Dyggve–Melchior–Clausen locus. J Med Genet 2012;49:455–461.

10. Cohn DH, Ehtesham N, Krakow D, et al. Mental retardation and abnormal skeletal development (Dyggve–Melchior–Clausen dysplasia) due to mutations in a novel, evolutionarily conserved gene. Am J Hum Genet 2003;72:419–428.

11. Ehtesham N, Cantor RM, King LM, et al. Evidence that smith-McCort dysplasia and Dyggve–Melchior–Clausen dysplasia are allelic disorders that result from mutations in a gene on chromosome 18q12. Am J Hum Genet 2002;71:947–951.

12. Sobreira N, Schiettecatte F, Valle D, et al. GeneMatcher: a matching tool for connecting investigators with an interest in the same gene. Hum Mutat 2015;36:928–930.

13. Monies D, Abouelhoda M, AlSayed M, et al. The landscape of genetic diseases in Saudi Arabia based on the first 1000 diagnostic panels and exomes. Hum Genet 2017;136:921–939.

14. Li H. Aligning sequence reads, clone sequences and assembly contigs with BWA-MEM. 2013.

15. Li H, Handsaker B, Wysoker A, et al. The sequence alignment/map format and SAMtools. Bioinformatics 2009;25:2078–2079.

16. McKenna A, Hanna M, Banks E, et al. The genome analysis toolkit: a MapReduce framework for analyzing next-generation DNA sequencing data. Genome Res 2010;20:1297–1303.

17. Koboldt DC, Zhang Q, Larson DE, et al. VarScan 2: somatic mutation and copy number alteration discovery in cancer by exome sequencing. Genome Res 2012;22:568–576.

18. Li H, Durbin R. Fast and accurate long-read alignment with burrows-wheeler transform. Bioinformatics 2010;26:589–595.

19. Kremer LS, Danhauser K, Herebian D, et al. NAXE mutations disrupt the cellular NAD(P)HX repair system and cause a lethal Neurometabolic disorder of early childhood. Am J Hum Genet 2016;99:894–902.

20. Kremer LS, L'hermitte-Stead C, Lesimple P, et al. Severe respiratory complex III defect prevents liver adaptation to prolonged fasting. J Hepatol 2016;65:377–385.

21. van der Auwera GA, Carneiro MO, Hartl C, et al. From FastQ data to high confidence variant calls: the genome analysis toolkit best practices pipeline. Curr Protoc Bioinformatics 2013;43:11.10.1–11.10.33.

22. Wang K, Li M, Hakonarson H. ANNOVAR: functional annotation of genetic variants from high-throughput sequencing data. Nucleic Acids Res 2010;38:e164.

23. Edgar RC. MUSCLE: multiple sequence alignment with high accuracy and high throughput. Nucleic Acids Res 2004;32:1792–1797.

24. Miller JA, Ding S-L, Sunkin SM, et al. Transcriptional landscape of the prenatal human brain. Nature 2014;508:199–206.

25. Kang HJ, Kawasawa YI, Cheng F, et al. Spatio-temporal transcriptome of the human brain. Nature 2011;478:483–489.

26. Penna I, Vella S, Gigoni A, et al. Selection of candidate housekeeping genes for normalization in human postmortem brain samples. Int J Mol Sci 2011;12:5461–5470.

27. Schwarz JM, Cooper DN, Schuelke M, et al. MutationTaster2: mutation prediction for the deep-sequencing age. Nat Methods 2014;11: 361–362.

28. Adzhubei IA, Schmidt S, Peshkin L, et al. A method and server for predicting damaging missense mutations. Nat Methods 2010;7: 248–249.

29. Choi Y, Chan AP. PROVEAN web server: a tool to predict the functional effect of amino acid substitutions and indels. Bioinformatics 2015;31:2745–2747.

30. Ng PC, Henikoff S. SIFT: predicting amino acid changes that affect protein function. Nucleic Acids Res 2003;31:3812–3814.

31. McLaren W, Gil L, Hunt SE, et al. The Ensembl variant effect predictor. Genome Biol 2016;17:122.

32. Richards S, Aziz N, Bale S, et al. Standards and guidelines for the interpretation of sequence variants: a joint consensus recommendation of the American College of Medical Genetics and Genomics and the zAssociation for Molecular Pathology. Genet Med 2015;17: 405–424.

33. Yu Y, Wang L, Jiu Y, et al. HID-1 is a novel player in the regulation of neuropeptide sorting. Biochem J 2011;434:383–390.

34. Rivinoja A, Pujol FM, Hassinen A, et al. Golgi pH, its regulation and roles in human disease. Ann Med 2012;44:542–554.

35. Dowland LK, Luyckx VA, Enck AH, et al. Molecular cloning and characterization of an intracellular chloride channel in the proximal tubule cell line, LLC-PK1. J Biol Chem 2000;275:37765–37773.

36. Dimitrov A, Paupe V, Gueudry C, et al. The gene responsible for Dyggve-Melchior-Clausen syndrome encodes a novel peripheral membrane protein dynamically associated with the Golgi apparatus. Hum Mol Genet 2009;18:440–453.

37. El Ghouzzi V, Dagoneau N, Kinning E, et al. Mutations in a novel gene Dymeclin (FLJ20071) are responsible for Dyggve-Melchior-Clausen syndrome. Hum Mol Genet 2003;12:357–364.

38. Dupuis N, Fafouri A, Bayot A, et al. Dymeclin deficiency causes postnatal microcephaly, hypomyelination and reticulum-to-Golgi trafficking defects in mice and humans. Hum Mol Genet 2015;24:2771–2783.

39. Denais C, Dent CL, Southgate L, et al. Dymeclin, the gene underlying Dyggve-Melchior-Clausen syndrome, encodes a protein integral to extracellular matrix and golgi organization and is associated with protein secretion pathways critical in bone development. Hum Mutat 2011;32:231–239.